New Journal of Physics
The open-access journal for physics

Structural and dynamical aspects of small three-dimensional spherical Coulomb clusters

S W S Apolinario[1], B Partoens and F M Peeters
Departement Fysica, Universiteit Antwerpen, Groenenborgerlaan 171, B-2020 Antwerpen, Belgium
E-mail: sergio.apolinario@ua.ac.be, bart.partoens@ua.ac.be and francois.peeters@ua.ac.be

New Journal of Physics **9** (2007) 283
Received 14 March 2007
Published 24 August 2007
Online at http://www.njp.org/
doi:10.1088/1367-2630/9/8/283

Abstract. An analysis of the structural and dynamical properties of small size three-dimensional clusters of classical charged particles confined in a spherical parabolic trap is presented. The ground state and the lowest metastable configurations are identified for Coulomb clusters consisting of $N = 4$–100 particles. The eigenmode frequencies are investigated both for clusters with Coulomb and screened Coulomb interparticle interaction. The breathing mode frequency is analytically determined and is found to be the highest energy eigenmode and independent of the number of particles for the case of Coulomb inter-particle interaction.

Contents

1. Introduction 2
2. Model and numerical approach 3
3. Fundamental characteristics of the GS and first MS 4
4. Normal modes 9
5. Summary and conclusions 17
Acknowledgment 17
Appendix. Static and dynamic properties of the GS and MS configurations of coulombic clusters 18
References 29

[1] Author to whom any correspondence should be addressed.

PII: S1367-2630(07)46207-3

1. Introduction

In 1934, Eugene Wigner predicted that a liquid to solid phase transition should occur in a three-dimensional (3D) electron gas at low temperature and density due to strong Coulomb repulsion [1]. This phase transition became known as Wigner crystallization and the solid phase as Wigner or Coulomb crystals. Wigner crystallization and properties of Coulomb crystals have been studied for decades in such a variety of systems as electron gas trapped on top of liquid helium [2], electrons trapped in quantum well structures [3], strongly coupled radio-frequency (rf) dusty plasmas [4], vortex clusters in an isotropic superfluid [5], laser-cooled trapped ion systems [6, 7], dusty plasmas [8], etc. Formation of ordered clusters with nested shells is expected to occur in expanding neutral plasmas [9, 10].

It is well known that an infinite Coulomb gas at low temperature self organizes in a body centered cubic lattice. Simulations have shown that the phase transition from order to a liquid state occurs at a well-defined temperature of $T \simeq 1/173$ in units of q^2/a_{WS} (where q is the charge and a_{WS} is the Wigner–Seitz radius, defined as $4/3\pi a_{\mathrm{WS}}^3 = 1/\rho$, with ρ the density). The situation is more complex for finite Coulomb crystals as shown by the pioneering works of Schiffer and co-workers. Numerical simulations have shown that the properties of a Coulomb crystal will depend both on the size and shape of the ion plasma, because of the importance of surface effects [11]–[15]. Finite clouds of ions show ordered structures with a different form of ordering. For instance, with a harmonic (and isotropic) confining potential that is representative for ion traps, cold particles form a cloud with a well-defined surface, constant macroscopic density, with well-defined concentric shells in the interior [11]. The surface layer and each (equally spaced) shell contain ions in a pattern of equilateral triangles. The triangles in the different shells cannot align perfectly; the pattern is reminiscent of the 'hexatic' ordering in liquid crystals. Such ordering of trapped ions has been observed both in computer simulations [15] and in the laboratory [16]. Ion clouds can also be confined in rf traps [17]. While the average confining field is a harmonic well, the particles undergo micromotion. The micromotion can also be viewed as due to some effective temperature. As long as those micromotions are small they do not have any influence on the configurations.

The first experimental investigation of spherical 3D dust plasma crystals consisting of micrometre-sized polymer particles was carried out recently [18]. It was found that small 3D strongly coupled charged particles in a spherical confining potential arrange themselves in a nested shell structure. In a subsequent publication on the same system [19] the sensitivity of the structural properties of the clusters to the type of interparticle forces was explored. By means of experiments, computer simulations, and theoretical analysis, they found that the number of shells are independent of the shielding while the shell occupation numbers are sensitive to screening which could be quantitatively explained by an isotropic Yukawa inter-particle interaction potential. The large size of the dust particles allows direct observation by simple video microscopy because dynamical processes occur on typical frequency scales of a few Hertz, quite unlike strongly coupled colloidal suspensions [20], where particle motion is heavily damped. Therefore, this system is ideally suited for studying the static and dynamics of strongly coupled matter with 'atomic resolution'. As mentioned by Arp *et al* [18] there are many directions of research with dusty plasmas, among them the dependence of phase transitions on system size, the formation of bcc order in the bulk of larger crystals, the role of fluctuations close to a phase transition or the exploration of elastic properties through fundamental types of vibrations.

In this paper, we address the case of small Coulomb clusters confined by a parabolic potential and interacting through a Coulomb or a screened Coulomb potential. Finite size effects are much more pronounced in this case with e.g. the occurrence of magic number configurations. One of the purposes of the present work is to elucidate the structural differences between the ground state (GS) and the lowest energy metastable state (MS). At high temperatures, transitions between different stable states occur. One of the most visited states during the dynamics is, of course, this lowest energy MS. We found that large clusters have a huge number of MS states with energies that are very close to each other. The latter fact strongly dilutes the weight of the lowest energy MS in the dynamics of the system. Here, we will limit ourselves to small clusters. Our investigation will be helpful in understanding the melting processes in small finite size Wigner crystals, both in theoretical [21] and experimental works. In contrast, previous investigations mostly concentrated on systems with a large number of particles ($N > 500$) [14, 18, 22, 23] or on static properties of the GS configurations [24]–[26]. In our report, the static and dynamic properties of MS for systems ranging from $N = 4$ to 100 particles are presented for the first time. To investigate the microscopic order in the particle configuration, we calculate the spherical Voronoi number associated with a specific polygon around a given particle. In this way we are able to obtain the number of nearest neighbors of each particle belonging to a specific shell. We show that for the same number of particles, the GS and MS configurations are in many cases structurally different; and we will classify those differences.

We present for the first time the eigenmode frequencies for the GS and the lowest energy MS. All the eigenmode frequencies which are independent of the number of particles are determined analytically. We show that the breathing mode frequency is an upper bound to the eigenmode frequency spectrum in systems interacting through a Coulomb potential. We found an approximate correlation between clusters with maximum (minimum) lowest nonzero eigenfrequency and the peak (minimum) in the second derivative of the binding energy with respect to N indicating the most stable (least stable) clusters. From this analysis, magic clusters are identified.

The paper is organized as follows. In the next section our model system and the methodology used to find stable configurations, eigenmode frequencies and their associated eigenvectors are given. In section 2, we deal with a system of classical particles interacting through a Coulomb interparticle potential. We investigate the static properties and present a Mendeleev-type table containing information about the structure of the GS. In addition the lowest energy MS configuration is determined and the three lowest nonzero frequencies for the MS and the GS configurations. In section 4, we investigate in more detail the dynamics of the previous systems. The eigenfrequencies and eigenvectors are determined both for Coulomb and screened Coulomb interparticle potential. Finally, in section 5, we present our conclusions.

2. Model and numerical approach

We study a 3D model system of N equally charged particles in a parabolic confinement potential and interacting through a repulsive potential. The Hamiltonian of the system is given by

$$H = \sum_{i=1}^{N} \tfrac{1}{2} m\omega_0 (x_i^2 + y_i^2 + z_i^2) + \sum_{j>i}^{N} \frac{q^2}{\epsilon} \frac{\exp(-|\mathbf{r}_i - \mathbf{r}_j|/\lambda)}{|\mathbf{r}_i - \mathbf{r}_j|}, \tag{1}$$

where m is the mass of the particle, $\mathbf{r}_i = (x_i, y_i, z_i)$ is the position of the ith particle, ω_0 is the frequency characterizing the confinement potential and λ is the screening length of the interparticle interaction potential. We can rewrite the Hamiltonian (1) in dimensionless form

$$H = \sum_{i=1}^{N}(x_i^2 + y_i^2 + z_i^2) + \sum_{j>i}^{N} \frac{\exp(-\kappa|\mathbf{r}_i - \mathbf{r}_j|)}{|\mathbf{r}_i - \mathbf{r}_j|}, \tag{2}$$

if we express the coordinates, energy, temperature and time, respectively, in the following units $r_0 = (q^2/\epsilon\gamma)^{1/3}$, $E_0 = \gamma r_0^2$, $T_0 = E_0 k_B^{-1}$ and $t_0 = \sqrt{2}/\omega_0$, where $\gamma = m\omega_0^2/2$. The dimensionless inverse screening length, $\kappa = r_0/\lambda$, is a measure of the range of the inter-particle interaction potential. All the results will be given in dimensionless units. It is clear from equation (2) that the GS is only a function of the number of charged particles N and the dimensionless screening length κ. To obtain the stable configurations we use the Monte Carlo simulation technique supplemented with the Newton method in order to speed up the computer program and to increase the accuracy of the found energy value (see [27] for details). By implementing a large number of different simulations starting from different random initial configurations we are confident that we found the GS configuration and the first MS as long as the number of particles N is not too large. Depending on the total number of particles, between several hundred to several thousand random initial configurations were generated.

The eigenfrequencies are the square root of the eigenvalues of the dynamical matrix

$$H_{\alpha\beta,ij} = \left.\frac{\partial^2 H}{\partial r_{\alpha,i}\partial r_{\beta,\,j}}\right|_{r_{\alpha,i}=r^n_{\alpha,i}}, \tag{3}$$

where $\{r^n_{\alpha,i}; \alpha = x, y, z; i = 1, \ldots, N\}$ are the positions of the particles in a stable configuration.

3. Fundamental characteristics of the GS and first MS

Any study of Wigner crystals without the knowledge of the details of the particles arrangements must of necessity be of a superficial nature. The particles of which Wigner crystals are composed are arranged in a highly regular way. It is this regularity, together with the attendant symmetry forced by the external confinement potential, that characterizes the crystalline state of finite systems. We present in table A.1 (see appendix), static and dynamic characteristics of the GS and the lowest energy MS for systems of particles interacting through a Coulomb potential and confined by an isotropic parabolic confinement. We considered systems ranging from $N = 4$ up to 100 particles. The main purpose of this table is to compile the most important crystallographic characteristics, which may be of general use to experimentalists and theoreticians. Table A.1 lists, from left to right, the number of particles in the system, its energy per particle, its configuration, the radius of the shells, the width of the shells, the value of the three nonzero lowest eigenfrequencies, and the number of particles per shell with 'x' nearest neighbors, as obtained by our Voronoi analysis. Except for $N = 4$–12 particles, which have only one stable state, table A.1 also lists the first MS.

The number of shells in the system depends on the total number of particles and in general the number of shells increases with the number of particles. From the third column of table A.1

we can see that the GS configuration of systems up to 12 particles consists of a single shell. Those configurations in fact form 3D regular polygons. From $N = 13$ to 60 the arrangement of particles in the GS configuration forms two shells except for the clusters with $N = 58$ and 59 particles, which respectively have the configurations (1, 12, 45) and (1, 12, 46), i.e. they form a two shell configuration with one extra particle in the center. The two shell configuration of the GS of $N = 60$ particles is unusual since it has less shells than the GS configuration of the $N = 58$ and 59 systems. This is a consequence of the fact that $N = 60$ has the highly symmetric configuration (12, 48) with a commensurate arrangement of the two shells resulting in a higher stability which is expressed in a large lowest (nonzero) eigenfrequency. For $61 < N \leqslant 100$ we have a three shell configuration as GS. We can formulate filling rules for the shells when the system is in the GS. For example, the maximum number of particles accommodated in systems with a single shell is 12 for the GS configuration. For larger systems, the extra particles form new shells in the system. Initially, for example for the case $N = 13$, the extra particle is placed in the center of the cluster. The number 12 also appears as an upper limit to the number of particles for the inner shell of the two-shell GS configuration. This can be seen when we go from $N = 57$ to $N = 58$ and $N = 60$ to $N = 61$. Similarly, we observe that 48 is the upper limit for the number of particles in the second shell for systems having two shells as observed for $N = 60$.

From the third column of table A.1, i.e. the column listing the configurations, it is clear that the GS and MS state configurations can differ in the number of shells or in the number of particles in each shell. For example, the system with $N = 9$ particles has the GS configuration with a single shell while its MS configuration has a two shell structure; the system with $N = 21$ particles has a different number of particles in the shell of its GS and MS configurations, respectively equal to 20 and 19. On the other hand, there are other systems, where the structural difference between GS and MS configurations is not related to a difference in the number of shells or in the number of particles per shell. This is the case for the systems: $N = 17$, 23, 24, 27, 28, 31–33, 35–39, 41–49, 52–54, 57, 59 and all systems larger than $N = 60$ particles with the exception of the systems $N = 80$, 82 and 91. Among the latter systems, some of them have structural differences between the GS and MS configurations due to differences in the number of particles per shell with 'x' nearest neighbors. This is the case for the systems: $N = 23$, 59, 73, 74, 76, 77, 83, 86, 87, 90, 97, 99 and 100. The latter fact is documented in the last five columns of table A.1. For example, for the GS configuration of the $N = 59$ system, the number of particles $N(x)$ in the third shell that has 'x' nearest neighbors is $N(3) = 0$, $N(4) = 0$, $N(5) = 12$, $N(6) = 34$ and $N(7) = 0$ and for the MS configuration it is $N(3) = 0$, $N(4) = 0$, $N(5) = 15$, $N(6) = 28$ and $N(7) = 3$. As an example, we show in figures 1(a) and (b) the particles on the outermost shell of the GS and MS configurations of the system with $N = 59$ particles. From figure 1(a) we can clearly identify particles with five and six nearest neighbors as indicated in table A.1. From figure 1(b), we can see the three particles, in black, each having seven nearest neighbors. We notice that the particles in black are relatively close to each other while the other particles with five and six nearest neighbors are distributed through the rest of the cluster. While for this latter system the particle packing in the third shell differs in the GS and MS configurations, for the system with $N = 86$ particles, the structural difference is found to occur in the second shell. There, the arrangement of particles for the GS configuration is $N(5) = 12$ and $N(6) = 9$ while for the MS configuration it is $N(4) = 1$, $N(5) = 10$ and $N(6) = 10$.

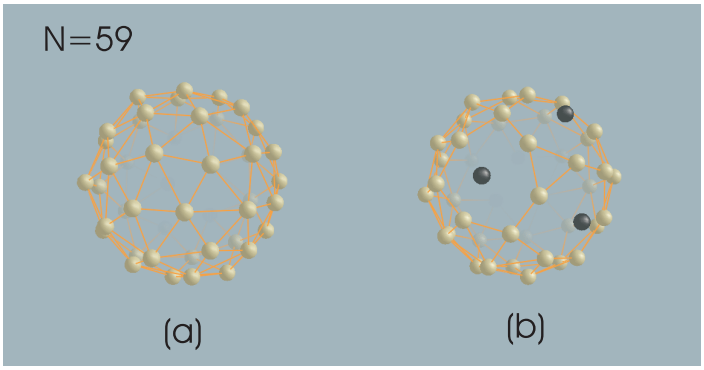

Figure 1. Particle arrangement on the outermost shell for the GS (a) and lowest energy MS state (b) configurations of the system with $N = 59$ particles. In order to improve visualization bounds between neighboring particles are drawn except for the seven coordinated particles in (b) which are drawn in black color.

The present results for the GS energy and the corresponding configuration agrees with those recently found in [25]. In the later work, the results for $N = 87$ were missing. In [26], the metastable configurations were given for $N = 2$ up to $N = 22$. There are a few differences with our results. The $N = 9$ and $N = 19$ clusters were found not to exhibit a MS while in our work we found a MS.

An interesting concept in the description of a finite size Wigner crystal is that of the width of the shell—in general the bigger the system, the larger the shell width is (see fifth column of table A.1). In fact large systems have a more compact internal structure while in small clusters particles accommodate themselves in shells with well-defined radius. Without taking this fact into account it would not be possible to understand the basic effects which come into play in different finite size Wigner crystals.

Figure 2 shows the dependence of the energy difference between the first MS and the GS configuration as function of the total number of particles when the configurations have different (black open squares) or the same (red squares) number of particles per shell. For small systems, $N \leqslant 56$, the energy difference indicated by the black open squares is larger than those of the red squares except in the case of $N = 29$ particles. It shows that the transition which involves changing the number of particles per shell has higher energy than the one which differs only by the arrangement of particles in a shell. As the number of particles increases the energy difference between the two types of configurations diminishes. This is a consequence of the fact that in larger systems the distance between particles belonging to distinct shells is small, since the shell's width is large and then, of course, the energy cost to move one particle from one shell to another will also be small. Note that the overall energy difference $E_2 - E_1$ decreases with increasing system size. Thus for large systems the ground and the lowest energy metastable configurations differ themselves by slight changes in the position of particles belonging to the same shell. The larger the system, the larger the number of particles in the outer shell and the larger the width of the shells. Consequently, as shown in figure 3, which displays the number of MS for clusters between $N = 4$ up to 100 particles, a larger system has many more stable configurations than a small one. For $N > 20$ the number of stable states increases exponentially. For N beyond 60 we are not 100% sure that we found all MSs because of the finite computational time.

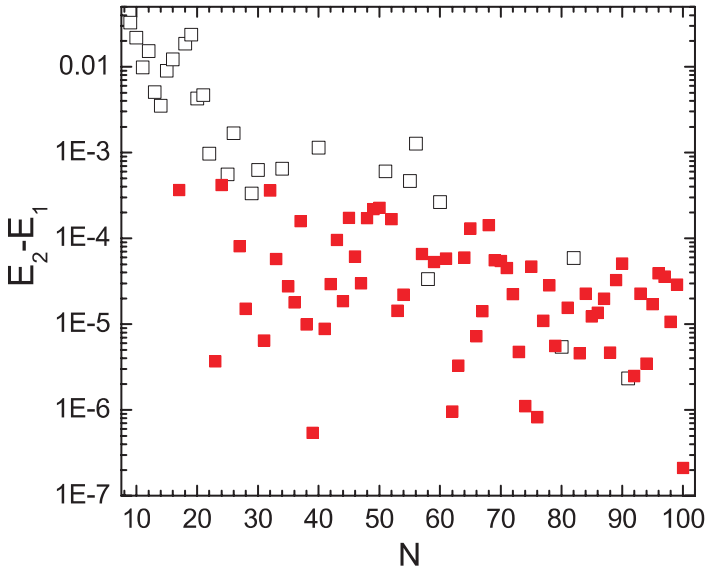

Figure 2. Energy difference between the first MS and the GS as function of the number of particles N when the configurations have different (black open squares) or the same (red squares) numbers of particles per shell.

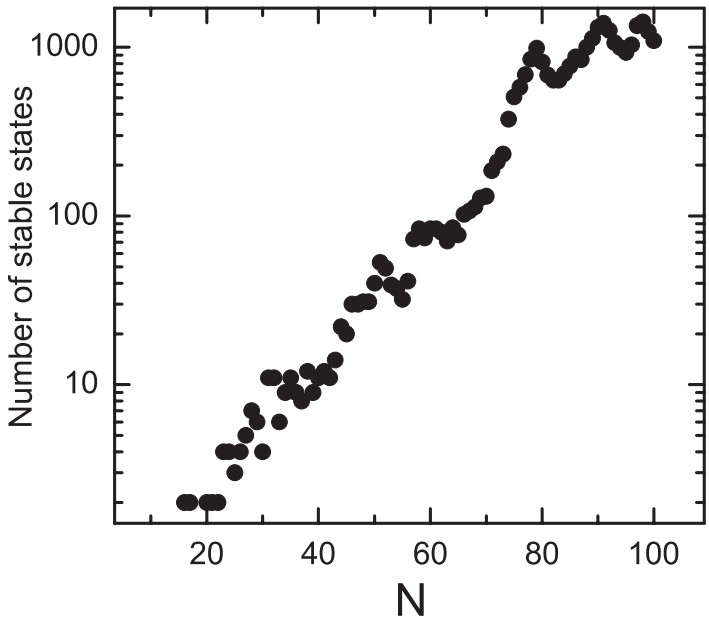

Figure 3. Number of stable states, i.e. the GS and MS state configurations, found for systems ranging from $N = 4$ up to 100 particles.

Two-dimensional systems of repulsive particles most efficiently self organize in a simple lattice of triangles. Such 6-fold coordinated triangular lattices [28] cannot be wrapped on a sphere surface without the introduction of extra defects. The topological characteristic of the arrangement of particles on the surface of a sphere can be characterized by their topological or

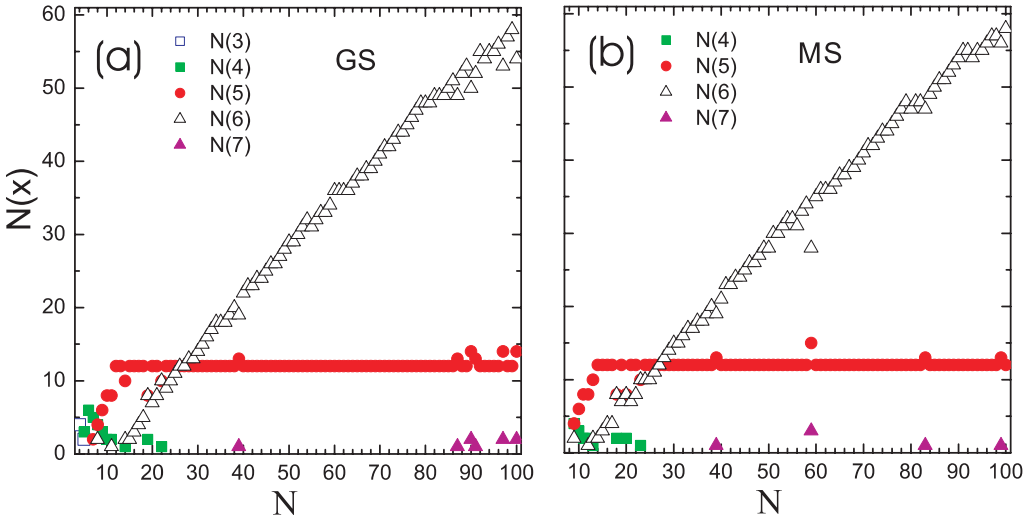

Figure 4. The number of particles in the outermost shell, $N(x)$, having x nearest neighbors in this shell, as function of the total number of particles for the GS (a) and the lowest energy MS (b) configuration.

disclination charge, q, which is the departure of their coordination number c from the preferred coordination number 6 ($q = 6 - c$). A classic theorem by Euler [29, 30] shows that the total disclination charge of any triangulation of the sphere must be 12. As the number of particles on the sphere grows, isolated charge $q = 1$ topological defects are predicted to produce too much strain [31], although this does not contradict Euler's theorem since the total defect charge is still 12. In order to explain the periodic table in terms of rigid spheres, nearly 100 years ago Thomson [32] attempted to determine the minimum energy configuration of repulsive particles lying on the surface of a sphere. Similar problems pervade in a wide range of fields such as multi-electron bubbles in superfluid helium [33], virus morphology [34] and protein s-layers [35, 36].

We determined the number of nearest neighbors for each particle in the outermost shell for systems ranging from $N = 4$ to $N = 100$. Similar results were given in [25] for $N = 2 \rightarrow 22$ and in [26] for $N = 2 \rightarrow 160$ which were limited to the GS configuration. The results are displayed in the last five columns of table A.1. Figures 4(a) and (b) display respectively for the GS and the lowest energy MS configurations the dependence of $N(x)$ on the total number of particles for the outermost shell. Notice that the MS and GS configurations for systems larger than $N = 11$ particles share the same properties concerning the arrangement of particles on the shell. The number of particles with five nearest neighbors saturates around 12 while the number of particles with six nearest neighbors increases linearly with the total number of particles. Both the GS and the MS configuration have in their outer shell a total defect charge equal to 12. For example, the outermost shell of the GS configuration with $N = 97$ has a total charge defect equal to 12 since the defect charge $q = -2$ associated with the two 7-fold-coordinated defects is canceled by the charge $q = +2$ due to the excess of two defects of 5-fold-coordination. On the other hand, particles with three nearest neighbors are only possible in the GS configuration of systems with $N = 4$ and 5 particles which do not exhibit any MS configuration. It is also seen in both the MS and GS configurations that mostly in small size systems, particles in the outermost shell can have a small number of particles with only three or four nearest neighbors.

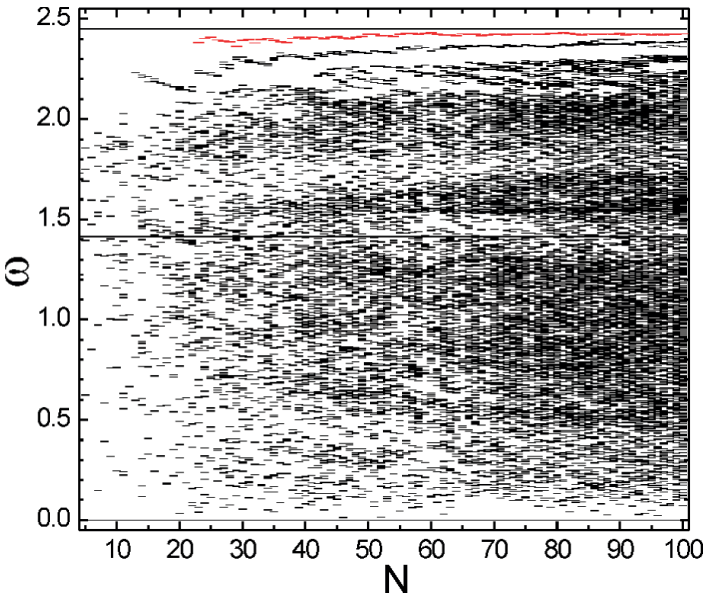

Figure 5. Eigenfrequency in units $\omega_0/\sqrt{2}$ of the normal modes for the GS configuration of the pure Coulomb system as function of the particle number N. The second highest frequency is indicated by red ticks.

4. Normal modes

Here, we discuss the excitation spectrum corresponding to the GS configuration of systems of isotropically confined particles interacting both through a Coulomb and screened Coulomb interparticle potential. This spectrum is shown in figure 5 for the Coulomb interacting system, as function of the number of particles for N ranging from 4 to 100. The eigenfrequency in this figure is in units of $\omega_0/\sqrt{2}$. Notice that there are three eigenfrequencies which are independent of N: (i) for any axial symmetric confinement potential the system as a whole can rotate, which gives a 3-fold degenerate eigenmode vibration with frequency $\omega = 0$. Figure 6(a) shows the eigenvectors associated with this mode for the system with $N = 12$ particles. (ii) There is a 3-fold degenerate vibration of the center of mass with frequency $\omega = \sqrt{2} = 1.4142$. This is an expression of Kohn's theorem for a finite size system. Figure 6(b) displays the eigenvectors associated with this mode for the system with $N = 12$. (iii) The third eigenfrequency corresponds to a vibration of the mean square radius $R^2 = \sum_i (x_i^2 + y_i^2 + z_i^2)$ with frequency $\omega = \sqrt{6} = 2.4495$. This mode is called a breathing mode and is illustrated in figure 6(c) for the system with $N = 12$ particles. Such a mode was also obtained from the cold fluid theory [37], where there it was referred to as the monopole mode. The breathing mode frequency is the highest frequency mode and is independent of the number of particles (figure 5). This is in contrast to 2D confined systems of particles interacting through a Coulomb potential where the breathing mode frequency is not the highest frequency mode. The present situation is similar to the case of logarithmic interacting particles [38], confined by a 2D parabolic potential where also the breathing mode has the highest frequency. This is not very surprising because the Coulomb interaction of charged particles in a 2D world is logarithmic. In fact [38] showed that if Earnshaw's theorem [39] is valid for a given system then the largest radial restoring force will come solely from the external confinement potential. Consequently the breathing

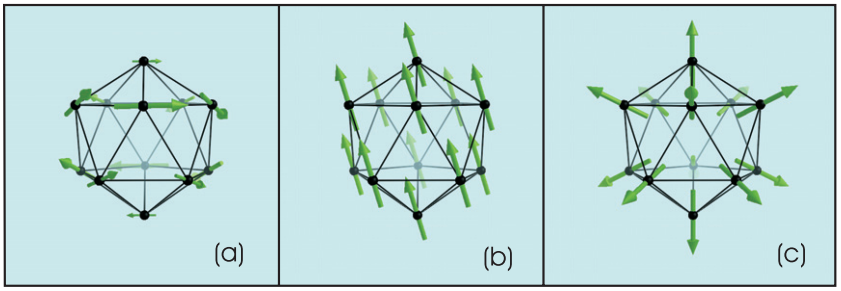

Figure 6. Visualization of the cluster structure and oscillation mode for the system with $N = 12$ particles. (a), (b) and (c) show respectively the eigenvectors of the rotational, center of mass and breathing modes. The arrows represent the eigenvectors, and the arrow's length is proportional to the amplitude of oscillation of the associated particle.

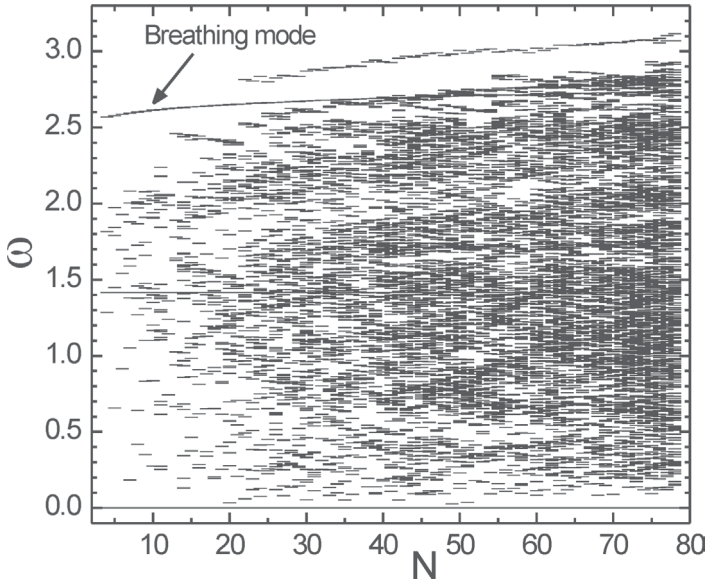

Figure 7. Eigenfrequency (in units of $\omega_0/\sqrt{2}$) of the normal modes for the GS configuration as function of the total number of particles for a systems of screened Coulomb potential with screening parameter $\kappa = 0.6$.

mode, in which motion of particles is mainly against the confinement potential, will have the largest frequency of oscillation. In this case the addition of particles in the system is only able to enhance slightly the breathing-like modes. In fact we can see (figure 5) that the value of the second largest frequency increases with the number of particles N and then approaches the value of the breathing mode frequency. However as expected by Earnshaw's theorem, the second largest eigenfrequency does not overtake the value of the breathing mode frequency.

Contrary to ion crystals, where particles interact via a pure Coulomb force, the microparticles in a dusty plasma are expected to interact through a Yukawa type pair potential. A typical value for the screening parameter is $\kappa = 0.6$ [19]. The eigenfrequency spectrum of the GS configuration of a Yukawa system with screening parameter $\kappa = 0.6$ and particle

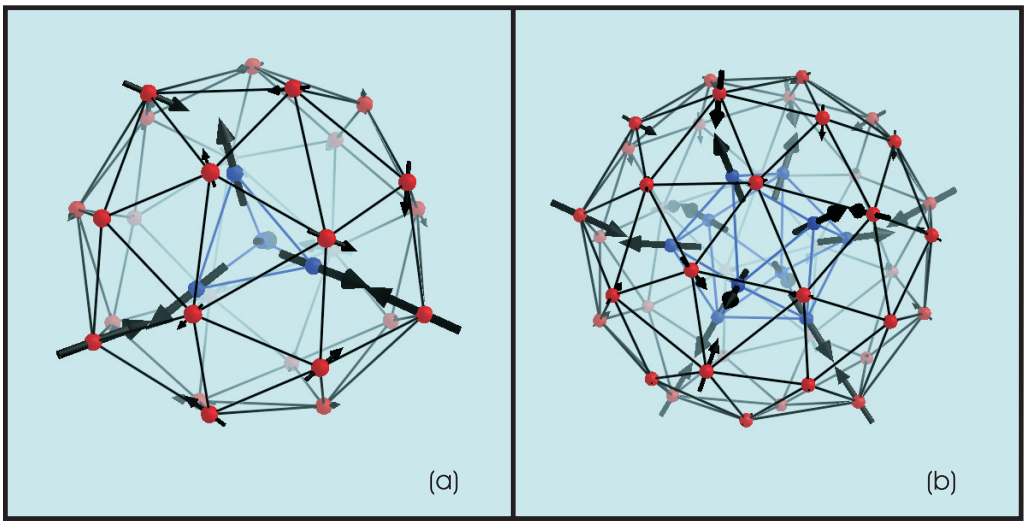

Figure 8. Eigenvectors of the normal mode of largest frequency for the screened Coulomb systems ($\kappa = 0.6$) with (a) $N = 30$ and (b) 50 particles. Particles in the external and internal shells are represented respectively by black and red balls. The arrows represent the eigenvectors of the specific normal mode, and the arrow's length is proportional to the amplitude of oscillation of the associated particle. Bonds are drawn between first neighboring particles to improve visualization.

number varying from $N = 4$ up to 80 is shown in figure 7. For screened interaction ($\kappa \neq 0$), the frequency of the rotational and center of mass mode are unaffected since they do not involve a relative particle motion. In contrast, the frequency of the breathing mode will depend on κ and N and is not necessarily the highest frequency mode. The breathing mode is indicated in figure 7 (black arrow). We can see that for $N \geqslant 22$ there starts to appear frequencies with larger values than the breathing mode frequency. With increasing κ, the radial position r_i of the particles in the isotropic confinement well is reduced, the clusters become smaller due to the reduced Coulomb repulsion. With reduced distance, the curvature of the Debye–Hückel potential increases more strongly than the confinement potential force, which in turn leads to the observed increase of the mode frequency (compare figure 5, for $\kappa = 0$, and figure 7, for $\kappa = 0.6$). As the number of particles increases eventually some of those modes obtain larger frequency than the breathing mode frequency (see figure 7). We show in figures 8(a) and (b), respectively the eigenvectors of the normal mode of largest eigenfrequencies for the systems with $N = 30$ and 50 particles. These modes are characterized by (i) a radial oscillation of particles in the internal shell, (ii) the closest particle in the external shell to a given particle in the internal shell also oscillates radially but out of phase with the oscillation of particles in the internal shell, and (iii) the rest of the particles in the external shell have a smaller amplitude of oscillation which is mainly directed tangentially to the shell surface. Such a motion involves a strong change of interparticle distance between some pairs of particles belonging to the internal and external shells, which results in strong restoring forces and thus a high frequency of the mode. Such normal modes were studied experimentally in 2D finite screened Coulomb clusters [40]. In that case the mode of highest frequency is also dominated by a strong relative motion of particles and turned out to be no longer the breathing mode frequency.

Following [27, 41], the value of the center of mass mode can be obtained analytically. The Hamiltonian equation of motion yields

$$\dot{v}_{xi} = -2x_i + \sum_{j_{j\neq i}} \left(\kappa + \frac{1}{r_{ij}}\right) \frac{x_{ij}}{r_{ij}^2} \mathrm{e}^{-\kappa r_{ij}}, \tag{4}$$

where $x_{ij} = x_i - x_j$ and $r_{ij} = |\vec{r}_i - \vec{r}_j|^2$. We have the same for $\dot{v}_{yi}$ and $\dot{v}_{zi}$ and. The displacement of the center of mass $R_x = \sum_i x_i$ along the x-direction satisfies the differential equation

$$\frac{\mathrm{d}^2 R_x}{\mathrm{d}t^2} = \sum_i \dot{v}_{x_i} = -2R_x, \tag{5}$$

and the same for R_y and R_z. We conclude that the eigenfrequencies of the center of mass along the directions x, y and z are all equal to $w = \sqrt{2}$. This frequency is independent of the number of charged particles and of the inter-particle potential.

The breathing mode frequency can be obtained as follows. The mean square radius $R^2 = \sum_i (x_i^2 + y_i^2 + y_i^2)$ satisfies the following differential equation

$$\frac{\mathrm{d}^2 R^2}{\mathrm{d}t^2} = 2T - \sum_{i=1}^{N} (x_i^2 + y_i^2 + z_i^2) + 2 \sum_{j>i} \left(\kappa + \frac{1}{r_{ij}}\right) \mathrm{e}^{-krij}, \tag{6}$$

with $T = \sum_i (\dot{x}_i^2 + \dot{y}_i^2 + \dot{z}_i^2)$ the total kinetic energy. For the particular case $\kappa = 0$ the former equation reduces to

$$\frac{\mathrm{d}^2 R^2}{\mathrm{d}t^2} = -6R^2 + 2(T + H), \tag{7}$$

where now H is the Hamiltonian for the particular case under study. Thus the frequency of the breathing mode for systems of isotropically confined particles interacting through a Coulomb interparticle potential is $\omega = \sqrt{6}$ and is independent of the number of particles.

Recently, dynamical properties of Coulomb clusters were studied experimentally in which a selective excitation of modes was performed [42, 43]. The experimental technique was applied to 2D clusters and should be extended to 3D [42]. In such systems a normal-mode analysis can become one of the key diagnostics for determining the particle charge and shielding effects. The first step in this direction is the characterization of the normal modes. Beside the three well known oscillation modes, i.e. rotational mode, center of mass mode and breathing mode, we call to attention the presence of another frequency, shown by the red data in figure 5, which is slightly smaller than the breathing mode frequency. This normal mode appears for systems having more than a single shell with one particle in the center ($N \geqslant 23$ particles). In order to characterize this mode we computed the averaged radial deviation of the eigenvectors, which characterizes the radial oscillation of the particles. This quantity is defined as

$$\delta_{\mathrm{r}} = \sum_{i=1}^{N} \frac{\vec{r}_i . \vec{v}_i}{|\vec{r}_i| . |\vec{v}_i|}, \tag{8}$$

where $\vec{r}_i$ and $\vec{v}_i$ are respectively the position vector and the eigenvector of the ith particle. Since δ_{r} is normalized, its maximum (minimum) value is $\delta_{\mathrm{r}} = 1(-1)$ and occurs when the vectors $\vec{r}_i$ and $\vec{v}_i$ are parallel (antiparallel) for all particles. Results are shown in figure 9,

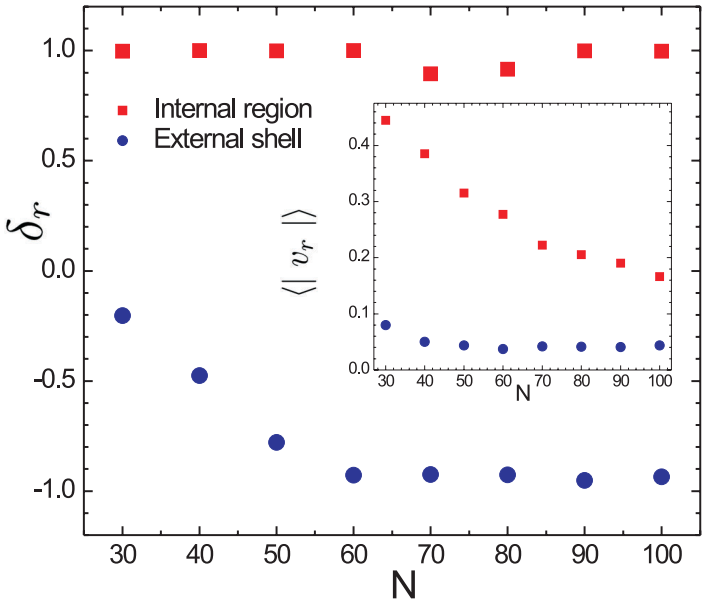

Figure 9. Averaged radial deviation of the eigenvectors δ_r calculated in the internal region of the cluster (red squares) and in the external shell (blue dots) as function of N. In the inset, the average length of the radial component of the eigenvector are displayed for both the internal region (red squares) and the external shell (blue dots).

for δ_r computed for the external shell (blue dots) and for the region enclosed by the external shell (red squares). The oscillations of the particles in the center of the cluster are mainly along the radial direction ($\delta_r \approx 1$). Note that the oscillation of particles in the external shell exhibits two different behaviors. For small size systems ($N < 40$), δ_r is small and particles oscillate mainly parallel to the shell while for larger systems ($N > 50$), δ_r is larger and particles oscillate mainly perpendicular to the shell. The simple determination of the direction of oscillation of particles is not enough to provide a satisfactory outline of this oscillation mode. To characterize the oscillation mode it is equally important to know the relative motion between particles as well as their amplitude of oscillation. Note that the value of δ_r has an opposite sign when calculated in the distinct regions. This fact shows that the oscillation performed by particles in the internal region is out of phase with the oscillation of particles on the external shell. The length of the eigenvectors is proportional to the amplitude of oscillation of the particles. The average of the eigenvector's length is shown in the inset of figure 9 when calculated in the internal region (red squares) and in the external shell (blue dots). We can conclude that particles in the internal region oscillate with larger amplitude than particles on the external shell.

Schweigert and Peeters [27] showed that for 2D systems normal mode analysis is an efficient tool to predict the stability of the cluster. This confirmed the existence of magic clusters in 2D systems: magic clusters were shown to have large values of the first nonzero frequency while non-stable clusters were found to have small values. In order to test if the lowest nonzero eigenfrequencies give similar information concerning the stability of 3D clusters, we computed for the first time the normal modes of 3D isotropic systems. Figure 10 displays the value of the first nonzero frequencies (blue square, left axis) for systems varying from $N = 4$ to 100 particles.

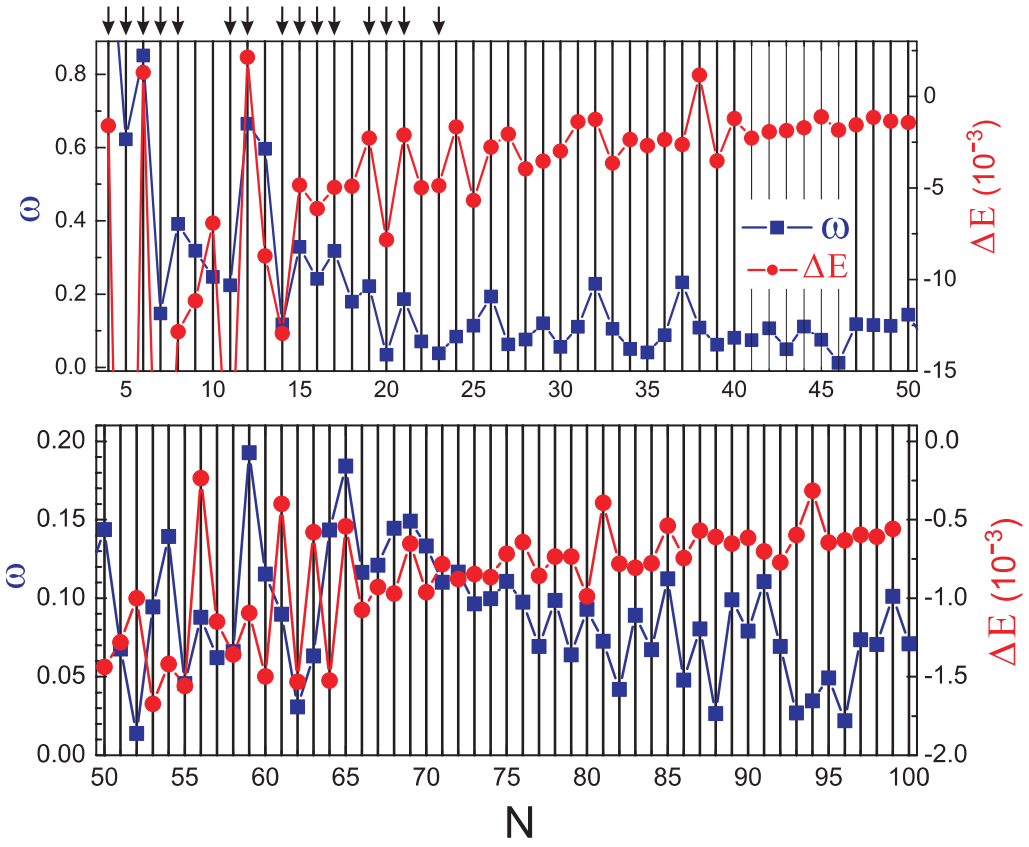

Figure 10. (a) and (b) display the first nonzero frequency (left axis and blue square) and the second derivative of the binding energy (right axis and red circle) as function of the number of particles.

The stability of 3D clusters was investigated previously through the calculation of the second derivative of the binding energy with respect to N in [26, 44], which is defined [45] by

$$\Delta E = E(N+1) + E(N-1) - 2E(N), \tag{9}$$

where $E(N)$ is the GS energy of a N-particle cluster. The binding energy (red dots, right axis) as function of the total number of particles for systems ranging from $N = 4$ up to 100 particles is shown in figure 10. The GS configuration of systems with $N = 4, 6, 10, 12, 19, 32, 38, 56$ [44] and $N = 81, 94$ [26] were classified as magic clusters. We can see that for those systems there is a pronounced peak in the value of ΔE. From figure 10 we can see that in many situations the maxima and minima in the value of ΔE and those in the first nonzero eigenfrequency coincide for small systems with only a single shell ($N < 22$). Those systems are indicated by arrows on the top of figure 10(a). On the other hand, such coincidences in the maxima and minima is not that evident for larger systems. Furthermore, the system with $N = 13$ can also be identified as a magic number cluster based on our normal mode analysis. However, it was not classified as a magic cluster in [26, 44]. In fact not all magic clusters can be revealed by the analysis of the binding energy, especially when there are two magic clusters with similar structure but differing only by one single particle. In other words, the energy difference of the system with $N = 13$ particles is negative due to a pronounced decrease of energy found in the magic cluster with $N = 12$ particles.

In order to understand why there is correspondence between a peak in ΔE and a high first non-zero eigenfrequency for 3D clusters with a single shell, and no correspondence for larger 3D clusters, it is important to consider typical eigenmodes corresponding to these eigenfrequencies. Figure 11 shows in sequence from (a) to (h) the eigenvectors associated to the lowest nonzero frequency for the systems with $N = 6$, 12, 13, 23, 28, 29, 36 and 60 particles. Those systems were chosen because they have different numbers of particles in the inner shell. In the external shell the 4-, 5-, and 6-fold particles are represented respectively by gray, black and orange balls. Particles in the inner shell are indicated by red balls. The arrows indicate the direction of oscillation while their lengths are proportional to the amplitude of oscillation of each associated particle. For the systems with $N = 6$ and 12 particles (figures 11(a) and (b)) we notice that their eigenvectors are mainly directed tangentially to the surface of the shell of the cluster. We call this sort of mode an intra-shell motion. The large value of the eigenfrequencies for the systems with $N = 6$ and 12 particles indicates that these magic clusters have large mechanical resistance against intra-shell diffusion. The eigenfrequency of the system with $N = 13$ particles is $\omega = 0.5966$ which is comparable to the eigenfrequency of the system with $N = 12$ particles. Figure 11(c) displays the eigenvectors for the first nonzero frequency of the system with $N = 13$ particles, which is similar to the mode of the system with $N = 12$ particles, i.e. an intra-shell motion. This fact is not surprising since the system with $N = 13$ particles has exactly the same arrangement of particles as for the system with $N = 12$ but with one extra particle in the center. This confirms why the system with $N = 13$ particles is also a magic cluster. For small systems, i.e. the ones with only one shell, we found that the normal mode corresponding to the lowest nonzero frequency corresponds to an intra-shell motion. However, for larger clusters the situation is more complex. Figures 11(d)–(h) display the eigenvectors, respectively, for the systems with $N = 23$, 28, 29, 36 and 60 particles. Notice that particles in the external as well as in the inner shell have oscillation amplitudes different from zero. A careful look at the eigenvectors associated with particles in the inner shell shows that they have a rotational motion while the motion of the particles in the external shell corresponds to an intra-shell diffusion of the particles. Thus the normal mode of lowest frequency for larger systems is a mixed mode, i.e. a combination of rotation and diffusion, respectively played by particles in the inner and external shells.

With this information we can understand why there is a correspondence between a peak in ΔE and a high first nonzero eigenfrequency for 3D clusters with a single shell, and no correspondence anymore for larger 3D clusters. This is not a surprise since in 3D systems the total energy can be reduced via two different processes, i.e. the arrangement of particles in the shells or between shells. The shell of the cluster can be thought of as a quasi 2D system. Then one expects that by a symmetric triangular arrangement of particles in the shell the energy can be reduced. Such arrangement in the shell may increase the resistance of the cluster against intra-shell diffusion but has nothing to do with the resistance against inter-shell motion. With this picture the cluster should then remain with a small first nonzero frequency for the rotation mode, even if the total energy is small due to a more symmetric triangular arrangement in the shell. The fact that the motion corresponding to the first nonzero frequency is a mixed one is the main reason of the disagreement found between the maxima and minima of ΔE and the first nonzero frequency for large systems. This picture is different from the one found in a 2D Wigner crystal since in that situation the normal mode corresponding to the first nonzero frequency is always an inter-shell rotation mode, i.e. there are no mixed modes. Furthermore, magic clusters are the ones where particles arrange themselves in a more triangular arrangement. This arrangement

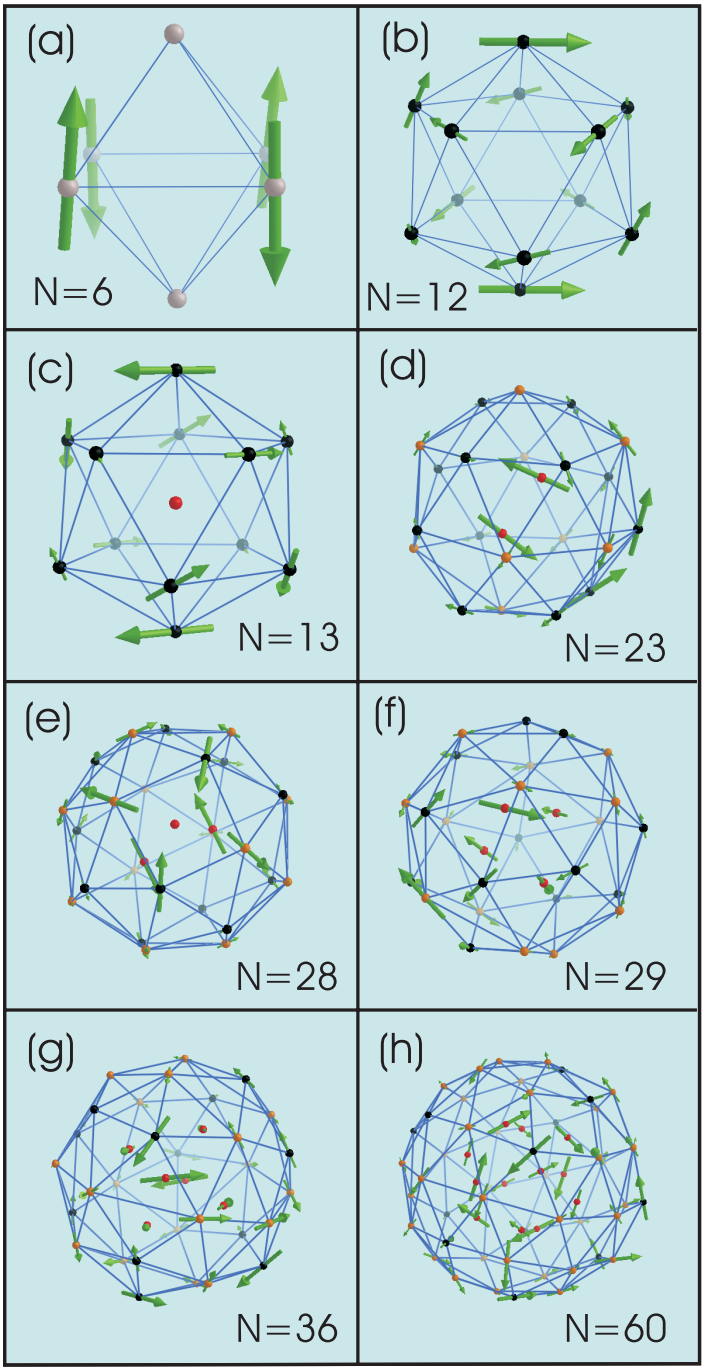

Figure 11. Visualization of the cluster structure and oscillation mode. For the external shell 4-, 5- and 6-fold particles are represented, respectively, by gray, black, and orange balls. Particles in the internal shell are represented by red balls. The arrows represent the eigenvectors associated with the lowest nonzero frequency, and the arrow's length is proportional to the amplitude of oscillation of the associated particle.

increases the value of the first nonzero frequency and decreases the total energy of 2D systems. That is why in 2D systems the magic clusters were successfully identified both via a normal mode analysis and energy calculations [45, 27]. We can conclude that in 3D systems the energy difference and the normal mode analysis give complementary information.

5. Summary and conclusions

We presented the results of a detailed numerical simulation of the configuration of the GS and the lowest energy MS configuration, and the spectrum of normal modes of classical 3D clusters with isotropic parabolic confinement. The confined particles interact through a repulsive potential such as Coulomb or screened Coulomb interparticle potential. For small systems the structural differences between the GS and MS configuration are mostly due to a different number of shells or different number of particles per shell. As the total number of particles increases the energy difference between GS and MS configuration decreases and the structural difference between them are often due to a different arrangement of the same number of particles in the shells.

The eigenmode frequencies are investigated both for Coulomb and screened Coulomb interparticle potential. Both small and larger systems satisfy Euler's theorem and the total topological charge defect is 12. For larger systems the appearance of negative defect charge (7-fold correlation defect) is compensated by an excess of positive charge due to defects with 5-fold coordination number. The breathing and the center of mass mode frequencies are analytically determined and both are independent of the number of particles. The breathing mode has the highest frequency value for the case of a Coulomb interparticle interaction potential system while this is no longer true for systems of confined particles interacting through a Yukawa potential. In fact the breathing mode has the highest frequency both for 2D and 3D parabolic confined systems when the interparticle interacting potential is given by the solution of the Poisson equation. In the present work, the Coulomb interaction is the solution of the Poisson equation while for a 2D system its solution is a logarithmic potential. We found a satisfactory relation between the appearance of maximum and minimum in the lowest nonzero eigenfrequency and in the second derivative of the binding energy as function of N for small clusters ($N < 23$) which indicates the most and least stable clusters. Such correspondence is not seen in larger clusters due to the fact that there the normal mode of the first nonzero frequency becomes a mixed mode with a rotational and intra-shell motion component.

Acknowledgment

This work was supported by the Flemish Science Foundation (FWO-Vl).

Appendix. Static and dynamic properties of the GS and MS configurations of coulombic clusters

Table A.1. From left to right: the number of particles in the system, its energy per particle, its configuration, the radius of the shell (r), the width of the shell ($\Delta(r)$), the value of the three nonzero lowest eigenfrequencies (f_i, $i = 1, 2, 3$), and the number of particles per shell with x nearest neighbors where x varies from 3 to 7.

N	E/N	Configuration	r	$\Delta(r)$	f_1	f_2	f_3	$N(3)$	$N(4)$	$N(5)$	$N(6)$	$N(7)$
2	0.7500000	2	0.5000	0.0000	1.4142	1.4142	1.4142	–	–	–	–	–
3	1.3103707	3	0.6609	0.0000	1.4142	1.4142	1.4142	–	–	–	–	–
4	1.7858262	4	0.7715	0.0000	1.2247	1.2247	1.4142	4	–	–	–	–
5	2.2451872	5	0.8651	0.0181	0.6226	0.6226	1.3954	2	3	–	–	–
6	2.6540390	6	0.9406	0.0000	0.8517	0.8517	0.8517	–	6	–	–	–
7	3.0641858	7	1.0106	0.0277	0.1472	0.1472	0.9726	–	5	2	–	–
8	3.4434094	8	1.0714	0.0000	0.3916	0.3916	0.5842	–	4	4	–	–
9	3.8097820	9	1.1269	0.0126	0.3185	0.3185	0.7584	–	3	6	–	–
	3.8425262	1,8	0.0000	–	0.2235	0.3348	0.3348	–	–	–	–	–
			1.2004	0.0000				–	4	4	–	–
10	4.1649900	10	1.1783	0.0131	0.2467	0.2467	0.7600	–	2	8	–	–
	4.1869791	1,9	0.0000	–	0.2719	0.2719	0.5719	–	–	–	–	–
			1.2453	0.0060				–	3	6	–	–
11	4.5132754	11	1.2265	0.0353	0.2243	0.2409	0.5546	–	2	8	1	–
	4.5231515	1,10	0.0000	–	0.2116	0.2116	0.6566	–	–	–	–	–
			1.2878	0.0070				–	2	8	–	–
12	4.8389665	12	1.2700	0.0000	0.6655	0.6655	0.6655	–	–	12	–	–
	4.8543111	1,11	0.0178	–	0.1992	0.2149	0.4765	–	–	–	–	–
			1.3286	0.0166				–	2	8	1	–
13	5.1667983	1,12	0.0000	–	0.5966	0.5966	0.5966	–	–	–	–	–
			1.3659	0.0000				–	–	12	–	–
	5.1718595	13	1.3130	0.0333	0.1311	0.1915	0.3391	–	1	10	2	–
14	5.4859154	1,13	0.0071	–	0.1176	0.1703	0.3059	–	–	–	–	–
			1.4033	0.0195				–	1	10	2	–
	5.4894163	14	1.3527	0.0000	0.3624	0.3624	0.4466	–	–	12	2	–
15	5.7920942	1,14	0.0000	–	0.3289	0.3289	0.4074	–	–	–	–	–
			1.4383	0.0154				–	–	12	2	–
	5.8011249	15	1.3906	0.0000	0.2582	0.2688	0.2688	–	–	12	3	–
16	6.0934213	1,15	0.0000	–	0.2414	0.2414	0.2437	–	–	–	–	–
			1.4719	0.0134				–	–	12	3	–
	6.1056214	16	1.4266	0.0000	0.3342	0.3495	0.3495	–	–	12	4	–
17	6.3886098	1,16	0.0000	–	0.3175	0.3175	0.3175	–	–	–	–	–
			1.5042	0.0139				–	–	12	4	–
	6.3889747	1,16	0.0000	0.0195	0.2426	0.2426	0.3619	–	–	–	–	–
			1.5042	0.0000				–	–	12	4	–

Table A.1. (Continued.)

N	E/N	Configuration	r	$\Delta(r)$	f_1	f_2	f_3	$N(3)$	$N(4)$	$N(5)$	$N(6)$	$N(7)$
18	6.6788303	1,17	0.0000	–	0.1791	0.1791	0.1823	–	–	–	–	–
			1.5353	0.0012				–	–	12	5	–
	6.6974417	18	1.4941	0.0352	0.2416	0.2416	0.3803	–	2	8	8	–
19	6.9641459	1,18	0.0000	–	0.2221	0.2221	0.3532	–	–	–	–	–
			1.5654	0.0122				–	2	8	8	–
	6.9878240	19	1.5261	0.0405	0.0227	0.2542	0.3329	–	–	12	7	–
20	7.2471808	1,19	0.0002	–	0.0345	0.2372	0.3101	–	–	–	–	–
			1.5946	0.0176				–	–	12	7	–
	7.2514451	2,18	0.5400	0.0504	0.1052	0.1593	0.2511	–	–	–	–	–
			1.6285	0.1090				–	2	8	8	–
21	7.5223777	1,20	0.0000	–	0.1869	0.1869	0.4160	–	–	–	–	–
			1.6226	0.0108				–	–	12	8	–
	7.5270457	2,19	0.5403	0.0621	0.1475	0.2144	0.2345	–	–	–	–	–
			1.6557	0.1041				–	–	12	7	–
22	7.7954689	1,21	0.0007	–	0.0712	0.0870	0.1565	–	–	–	–	–
			1.6499	0.0182				–	1	10	10	–
	7.7964445	2,20	0.5321	0.0007	0.0094	0.0845	0.2349	–	–	–	–	–
			1.6821	0.1052				–	–	12	8	–
23	8.0635754	2,21	0.5302	0.0000	0.0389	0.0627	0.1642	–	–	–	–	–
			1.7077	0.0927				–	–	12	9	–
	8.0635791	2,21	0.5303	0.0385	0.0901	0.0901	0.1692	–	–	–	–	–
			1.7077	0.1076				–	1	10	10	–
24	8.3268028	2,22	0.5260	0.0130	0.0842	0.1271	0.2047	–	–	–	–	–
			1.7326	0.0808				–	–	12	10	–
	8.3272196	2,22	0.5263	0.0000	0.0331	0.1201	0.1572	–	–	–	–	–
			1.7327	0.0854				–	–	12	10	–
25	8.5883607	2,23	0.5262	0.0000	0.1138	0.1138	0.2948	–	–	–	–	–
			1.7570	0.0978				–	–	12	11	–
	8.5889178	3,22	0.6958	0.0000	0.2054	0.2200	0.2200	–	–	–	–	–
			1.7849	0.1226				–	–	12	10	–
26	8.8442362	2,24	0.5241	0.0000	0.1934	0.1964	0.1964	–	–	–	–	–
			1.7805	0.0575				–	–	12	12	–
	8.8459235	3,23	0.6931	0.0195	0.1214	0.2303	0.2364	–	–	–	–	–
			1.8081	0.1219				–	–	12	11	–
27	9.0973346	3,24	0.6898	0.0166	0.0632	0.1058	0.2364	–	–	–	–	–
			1.8305	0.1045				–	–	12	12	–
	9.0974154	3,24	0.6895	0.0170	0.0683	0.1827	0.2391	–	–	–	–	–
			1.8305	0.0999				–	–	12	12	–
28	9.3483678	3,25	0.6889	0.0027	0.0765	0.1710	0.2133	–	–	–	–	–
			1.8525	0.1150				–	–	12	13	–
	9.3483829	3,25	0.6889	0.0215	0.1162	0.1361	0.2040	–	–	–	–	–
			1.8525	0.1289				–	–	12	13	–

Table A.1. (Continued.)

N	E/N	Configuration	r	$\Delta(r)$	f_1	f_2	f_3	$N(3)$	$N(4)$	$N(5)$	$N(6)$	$N(7)$
29	9.5954351	4,25	0.7987	0.0268	0.1203	0.1684	0.2458	4	–	–	–	–
			1.8992	0.1110				–	–	12	13	–
	9.5957698	3,26	0.6872	0.0055	0.0435	0.1723	0.1923	–	–	–	–	–
			1.8740	0.0964				–	–	12	14	–
30	9.8389647	4,26	0.7961	0.0311	0.0559	0.1627	0.1825	4	–	–	–	–
			1.9198	0.1109				–	–	12	14	–
	9.8395917	3,27	0.6841	0.0037	0.1424	0.1549	0.2055	–	–	–	–	–
			1.8950	0.1052				–	–	12	15	–
31	10.0795110	4,27	0.7926	0.0124	0.1114	0.1742	0.1847	4	–	–	–	–
			1.9399	0.1098				–	–	12	15	–
	10.0795174	4,27	0.7927	0.0208	0.0959	0.1931	0.1978	4	–	–	–	–
			1.9399	0.1165				–	–	12	15	–
32	10.3186788	4,28	0.7935	0.0000	0.2282	0.2282	0.2282	4	–	–	–	–
			1.9596	0.0882				–	–	12	16	–
	10.3190407	4,28	0.7912	0.0025	0.0908	0.1390	0.1828	4	–	–	–	–
			1.9597	0.1232				–	–	12	16	–
33	10.5565871	4,29	0.7914	0.0215	0.1059	0.1059	0.1714	4	–	–	–	–
			1.9791	0.1304				–	–	12	17	–
	10.5566443	4,29	0.7908	0.0092	0.0625	0.0997	0.1105	4	–	–	–	–
			1.9791	0.1208				–	–	12	17	–
34	10.7908419	4,30	0.7901	0.0000	0.0505	0.1399	0.1589	4	–	–	–	–
			1.9980	0.1052				–	–	12	18	–
	10.7914888	5,29	0.8867	0.0677	0.0303	0.1531	0.1568	2	3	–	–	–
			2.0200	0.1253				–	–	12	17	–
35	11.0227310	5,30	0.8859	0.0821	0.0413	0.1399	0.1672	2	3	–	–	–
			2.0381	0.1467				–	–	12	18	–
	11.0227585	5,30	0.8849	0.0820	0.0582	0.0719	0.0872	2	3	–	–	–
			2.0383	0.1448				–	–	12	18	–
36	11.2519226	6,30	0.9582	0.0000	0.0882	0.0882	0.2117	–	6	–	–	–
			2.0775	0.1018				–	–	12	18	–
	11.2519406	6,30	0.9576	0.0197	0.0748	0.0816	0.1126	–	6	–	–	–
			2.0775	0.1020				–	–	12	18	–
37	11.4787472	6,31	0.9585	0.0324	0.2319	0.2334	0.2334	–	6	–	–	–
			2.0947	0.1150				–	–	12	19	–
	11.4789060	6,31	0.9571	0.0480	0.0905	0.1492	0.2089	–	6	–	–	–
			2.0948	0.1228				–	–	12	19	–
38	11.7029516	6,32	0.9549	0.0000	0.1089	0.1490	0.1490	–	6	–	–	–
			2.1119	0.1166				–	–	12	20	–
	11.7029615	6,32	0.9546	0.0000	0.1070	0.1070	0.1070	–	6	–	–	–
			2.1119	0.0903				–	–	12	20	–
39	11.9283228	6,33	0.9549	0.0348	0.0621	0.1103	0.1316	–	6	–	–	–
			2.1289	0.1186				–	–	13	19	1
	11.9283233	6,33	0.9553	0.0387	0.0838	0.1437	0.1514	–	6	–	–	
			2.1288	0.1041				–	–	13	19	1

Table A.1. (Continued.)

N	E/N	Configuration	r	$\Delta(r)$	f_1	f_2	f_3	$N(3)$	$N(4)$	$N(5)$	$N(6)$	$N(7)$
40	12.1501629	6,34	0.9547	0.0253	0.0812	0.1198	0.1450	–	6	–	–	–
			2.1453	0.1282				–	–	12	22	–
	12.1513063	7,33	1.0280	0.1387	0.1032	0.1362	0.1663	–	5	2	–	–
			2.1641	0.1124				–	–	12	21	–
41	12.3707915	6,35	0.9538	0.0178	0.0751	0.0929	0.1339	–	6	–	–	–
			2.1618	0.1222				–	–	12	23	–
	12.3708003	6,35	0.9538	0.0095	0.0458	0.0954	0.1453	–	6	–	–	–
			2.1618	0.1276				–	–	12	23	–
42	12.5891393	7,35	1.0260	0.1218	0.1071	0.1321	0.1577	–	5	2	–	–
			2.1961	0.1298				–	–	12	23	–
	12.5891687	7,35	1.0264	0.1280	0.0601	0.1383	0.1617	–	5	2	–	–
			2.1961	0.1393				–	–	12	23	–
43	12.8055452	7,36	1.0252	0.0985	0.0498	0.1312	0.1877	–	5	2	–	–
			2.2119	0.1171				–	–	12	24	–
	12.8056408	7,36	1.0250	0.0903	0.1145	0.1300	0.1969	–	5	2	–	–
			2.2119	0.1261				–	–	12	24	–
44	13.0200779	8,36	1.0845	0.0370	0.1116	0.1178	0.1310	–	4	4	–	–
			2.2454	0.1386				–	–	12	24	–
	13.0200965	8,36	1.0848	0.0083	0.0529	0.1265	0.1412	–	4	4	–	–
			2.2454	0.1302				–	–	12	24	–
45	13.2329012	8,37	1.0845	0.0851	0.0758	0.1030	0.1208	–	4	4	–	–
			2.2603	0.1240				–	–	12	25	–
	13.2330752	8,37	1.0842	0.0472	0.1234	0.1454	0.1675	–	4	4	–	–
			2.2604	0.1555				–	–	12	25	–
46	13.4446015	8,38	1.0842	0.0826	0.0131	0.1450	0.1803	–	4	4	–	–
			2.2751	0.1129				–	–	12	26	–
	13.4446625	8,38	1.0833	0.0554	0.0649	0.1418	0.1447	–	4	4	–	–
			2.2752	0.1694				–	–	12	26	–
47	13.6544585	9,38	1.1391	0.1064	0.1185	0.1987	0.2025	–	3	6	–	–
			2.3066	0.1061				–	–	12	26	–
	13.6544883	9,38	1.1380	0.0960	0.0441	0.1211	0.1443	–	3	6	–	–
			2.3067	0.1277				–	–	12	26	–
48	13.8627620	9,39	1.1379	0.0892	0.1156	0.1582	0.1682	–	3	6	–	–
			2.3210	0.1235				–	–	12	27	–
	13.8629342	9,39	1.1372	0.0055	0.1039	0.1165	0.1165	–	3	6	–	–
			2.3212	0.1094				–	–	12	27	–
49	14.0699199	9,40	1.1371	0.0840	0.1137	0.1292	0.1552	–	3	6	–	–
			2.3351	0.1277				–	–	12	28	–
	14.0701384	9,40	1.1364	0.0457	0.0651	0.0651	0.0983	–	3	6	–	–
			2.3352	0.1305				–	–	12	28	–

Table A.1. (Continued.)

N	E/N	Configuration	r	$\Delta(r)$	f_1	f_2	f_3	$N(3)$	$N(4)$	$N(5)$	$N(6)$	$N(7)$
50	14.2757285	9,41	1.1372	0.0529	0.1438	0.1438	0.2186	–	3	6	–	–
			2.3490	0.1302				–	–	12	29	–
	14.2759561	10,40	1.1876	0.1061	0.0891	0.0925	0.0989	–	2	8	–	–
			2.3652	0.1101				–	–	12	28	–
51	14.4801010	10,41	1.1877	0.0859	0.0676	0.0910	0.2202	–	2	8	–	–
			2.3788	0.1292				–	–	12	29	–
	14.4807038	9,42	1.1363	0.0654	0.0759	0.1018	0.1526	–	3	6	–	–
			2.3629	0.1382				–	–	12	30	–
52	14.6831926	10,42	1.1875	0.0787	0.0140	0.1687	0.2052	–	2	8	–	–
			2.3922	0.1268				–	–	12	30	–
	14.6833601	10,42	1.1871	0.0747	0.0535	0.0851	0.1067	–	2	8	–	–
			2.3923	0.1269				–	–	12	30	–
53	14.8852839	10,43	1.1872	0.0824	0.0945	0.1074	0.1163	–	2	8	–	–
			2.4055	0.1520				–	–	12	31	–
	14.8852982	10,43	1.1872	0.0820	0.0689	0.1106	0.1510	–	2	8	–	–
			2.4055	0.1286				–	–	12	31	–
54	15.0857028	10,44	1.1872	0.0581	0.1393	0.1393	0.1671	–	2	8	–	–
			2.4186	0.1061				–	–	12	32	–
	15.0857248	10,44	1.1867	0.0620	0.0187	0.1361	0.1384	–	2	8	–	–
			2.4186	0.1485				–	–	12	32	–
55	15.2847026	12,43	1.2773	0.0250	0.0456	0.0456	0.1197	–	–	12	–	–
			2.4618	0.1086				–	–	12	31	–
	15.2851700	11,44	1.2356	0.1654	0.1349	0.1446	0.1660	–	2	8	1	–
			2.4465	0.1624				–	–	12	32	–
56	15.4821444	12,44	1.2770	0.0193	0.0879	0.0879	0.1185	–	–	12	–	
			2.4743	0.1110				–	–	12	32	–
	15.4834142	1,12,43	0.0407	–	0.0462	0.0462	0.0778	–	–	–	–	–
			1.3786	0.0463				–	–	12	–	–
			2.4878	0.1372				–	–	12	31	–
57	15.6793502	12,45	1.2763	0.0210	0.0622	0.1012	0.1334	–	–	12	–	–
			2.4869	0.1110				–	–	12	33	–
	15.6794160	12,45	1.2759	0.0031	0.0757	0.0757	0.1089	–	–	12	–	–
			2.4869	0.0953				–	–	12	33	–
58	15.8754062	1,12,45	0.0052	–	0.0661	0.0828	0.1215	–	–	–	–	–
			1.3765	0.0150				–	–	12	–	–
			2.5126	0.1406				–	–	12	33	–
	15.8754397	12,46	1.2766	0.0000	0.2012	0.2012	0.2012	–	–	12	–	–
			2.4992	0.0932				–	–	12	34	–
59	16.0701034	1,12,46	0.0000	–	0.1928	0.1928	0.1928	–	–	–	–	–
			1.3764	0.0000				–	–	12	–	–
			2.5247	0.1217				–	–	12	34	–
	16.0701563	1,12,46	0.0168	–	0.0722	0.0722	0.1448	–	–	–	–	–
			1.3771	0.0197				–	–	12	–	–
			2.5246	0.1294				–	–	15	28	3

Table A.1. (Continued.)

N	E/N	Configuration	r	$\Delta(r)$	f_1	f_2	f_3	$N(3)$	$N(4)$	$N(5)$	$N(6)$	$N(7)$
60	16.2637073	12,48	1.2755	0.0094	0.1154	0.1202	0.1202	–	–	12	–	
			2.5236	0.1007				–	–	12	36	–
	16.2639715	1,12,47	0.0036	–	0.0719	0.0934	0.1105	–	–	–	–	–
			1.3764	0.0197				–	–	12	–	–
			2.5368	0.1294				–	–	12	35	–
61	16.4558128	1,12,48	0.0041	–	0.0899	0.1262	0.1262	–	–	–	–	–
			1.3751	0.0063				–	–	12	–	–
			2.5488	0.1264				–	–	12	36	–
	16.4558710	1,12,48	0.0000	–	0.0628	0.0628	0.0628	–	–	–	–	–
			1.3752	0.0000				–	–	12	–	–
			2.5489	0.1046				–	–	12	36	–
62	16.6475197	1,13,48	0.0164	–	0.0308	0.1233	0.1538	–	–	–	–	–
			1.4134	0.0953				–	1	10	2	–
			2.5738	0.1612				–	–	12	36	–
	16.6475207	1,13,48	0.0249	–	0.0623	0.0981	0.1401	–	–	–	–	–
			1.4133	0.0715				–	1	10	2	–
			2.5739	0.1509				–	–	12	36	–
63	16.8376940	1,14,48	0.0047	–	0.0633	0.0949	0.0993	–	–	–	–	–
			1.4473	0.0762				–	–	12	2	
			2.5988	0.1408				–	–	12	36	–
	16.8376973	1,14,48	0.0037	–	0.0138	0.0897	0.1014	–	–	–	–	–
			1.4473	0.0742				–	–	12	2	–
			2.5988	0.1311				–	–	12	36	–
64	17.0272889	1,14,49	0.0019	–	0.1435	0.1435	0.1633	–	–	–	–	–
			1.4478	0.0758				–	–	12	2	–
			2.6101	0.1233				–	–	12	37	–
	17.0273485	1,14,49	0.0071	–	0.1001	0.1336	0.1504	–	–	–	–	–
			1.4475	0.0725				–	–	12	2	–
			2.6101	0.1266				–	–	12	37	–
65	17.2153608	1,14,50	0.0000	–	0.1842	0.1947	0.1947	–	–	–	–	–
			1.4477	0.0517				–	–	12	2	–
			2.6212	0.1197				–	–	12	38	–
	17.2154915	1,14,50	0.0026	–	0.0648	0.1149	0.1625	–	–	–	–	–
			1.4470	0.0784				–	–	12	2	–
			2.6215	0.1381				–	–	12	38	–
66	17.4028913	1,15,50	0.0059	–	0.1165	0.1246	0.1499	–	–	–	–	–
			1.4805	0.0846				–	–	12	3	–
			2.6453	0.1339				–	–	12	38	–
	17.4028985	1,15,50	0.0042	–	0.0667	0.1156	0.1299	–	–	–	–	–
			1.4804	0.0680				–	–	12	3	–
			2.6453	0.1289				–	–	12	38	–

Table A.1. (Continued.)

N	E/N	Configuration	r	$\Delta(r)$	f_1	f_2	f_3	$N(3)$	$N(4)$	$N(5)$	$N(6)$	$N(7)$
67	17.5893474	1,15,51	0.0046	–	0.1210	0.1384	0.1594	–	–	–	–	–
			1.4803	0.0724				–	–	12	3	–
			2.6563	0.1436				–	–	12	39	–
	17.5893617	1,15,51	0.0027	–	0.0809	0.0963	0.1458	–	–	–	–	–
			1.4802	0.0708				–	–	12	3	–
			2.6564	0.1412				–	–	12	39	–
68	17.7748744	1,16,51	0.0034	–	0.1446	0.1446	0.1748	–	–	–	–	–
			1.5123	0.0756				–	–	12	4	–
			2.6797	0.1201				–	–	12	39	–
	17.7750173	1,16,51	0.0155	–	0.1070	0.1310	0.1567	–	–	–	–	–
			1.5123	0.0957				–	–	12	4	–
			2.6797	0.1260				–	–	12	39	–
69	17.9594322	1,16,52	0.0010	–	0.1491	0.1768	0.1768	–	–	–	–	–
			1.5126	0.0968				–	–	12	4	–
			2.6903	0.1043				–	–	12	40	–
	17.9594876	1,16,52	0.0000	–	0.1329	0.1329	0.1329	–	–	–	–	–
			1.5130	0.0836				–	–	12	4	–
			2.6902	0.1055				–	–	12	40	–
70	18.1433383	1,16,53	0.0023	–	0.1333	0.1487	0.1622	–	–	–	–	–
			1.5119	0.0885				–	–	12	4	–
			2.7010	0.1228				–	–	12	41	–
	18.1433927	1,16,53	0.0057	–	0.0821	0.1361	0.1694	–	–	–	–	–
			1.5120	0.0928				–	–	12	4	–
			2.7010	0.1340				–	–	12	41	–
71	18.3262819	1,16,54	0.0084	–	0.1102	0.1590	0.1800	–	–	–	–	–
			1.5118	0.0791				–	–	12	4	–
			2.7116	0.1316				–	–	12	42	–
	18.3263270	1,16,54	0.0030	–	0.0962	0.1450	0.1653	–	–	–	–	–
			1.5115	0.0843				–	–	12	4	–
			2.7117	0.1371				–	–	12	42	–
72	18.5084443	1,17,54	0.0059	–	0.1167	0.1293	0.1315	–	–	–	–	–
			1.5423	0.0744				–	–	12	5	–
			2.7342	0.1505				–	–	12	42	–
	18.5084666	1,17,54	0.0073	–	0.0918	0.1218	0.1560	–	–	–	–	–
			1.5424	0.0797				–	–	12	5	–
			2.7342	0.1548				–	–	12	42	–
73	18.6897294	1,17,55	0.0047	–	0.0965	0.1287	0.1432	–	–	–	–	–
			1.5422	0.0724				–	1	10	6	–
			2.7445	0.1434				–	–	12	43	–
	18.6897341	1,17,55	0.0031	–	0.1061	0.1432	0.1773	–	–	–	–	–
			1.5420	0.0741				–	–	12	5	–
			2.7445	0.1568				–	–	12	43	–

Table A.1. (Continued.)

N	E/N	Configuration	r	$\Delta(r)$	f_1	f_2	f_3	$N(3)$	$N(4)$	$N(5)$	$N(6)$	$N(7)$
74	18.8701679	1,17,56	0.0088	–	0.0998	0.1439	0.1635	–	–	–	–	–
			1.5423	0.0640				–	2	8	7	–
			2.7546	0.1681				–	–	12	44	–
	18.8701690	1,17,56	0.0051	–	0.0698	0.1325	0.1501	–	–	–	–	–
			1.5421	0.0625				–	–	12	5	–
			2.7547	0.1790				–	–	12	44	–
75	19.0497421	1,18,56	0.0055	–	0.1108	0.1154	0.1461	–	–	–	–	–
			1.5717	0.1016				–	2	8	8	–
			2.7765	0.1401				–	–	12	44	–
	19.0497889	1,18,56	0.0058	–	0.0913	0.1288	0.1521	–	–	–	–	–
			1.5716	0.1007				–	2	8	8	–
			2.7765	0.1426				–	–	12	44	–
76	19.2286002	1,18,57	0.0000	–	0.0975	0.0975	0.1649	–	–	–	–	–
			1.5714	0.0562				–	–	12	6	–
			2.7865	0.1149				–	–	12	45	–
	19.2286011	1,18,57	0.0031	–	0.0628	0.1374	0.1574	–	–	–	–	–
			1.5717	0.0803				–	2	8	8	–
			2.7864	0.1317				–	–	12	45	–
77	19.4068165	1,18,58	0.0033	–	0.0693	0.1191	0.1454	–	–	–	–	–
			1.5714	0.0971				–	2	8	8	–
			2.7964	0.1390				–	–	12	46	–
	19.4068274	1,18,58	0.0056	–	0.0895	0.1175	0.1353	–	–	–	–	–
			1.5717	0.0958				–	–	12	6	–
			2.7964	0.1518				–	–	12	46	–
78	19.5841752	1,18,59	0.0046	–	0.0987	0.1108	0.1475	–	–	–	–	–
			1.5715	0.0732				–	–	12	6	–
			2.8063	0.1385				–	–	12	47	–
	19.5842034	1,18,59	0.0061	–	0.0972	0.1330	0.1460	–	–	–	–	–
			1.5714	0.0793				–	–	12	6	–
			2.8063	0.1373				–	–	12	47	–
79	19.7607999	1,18,60	0.0049	–	0.0641	0.1102	0.1913	–	–	–	–	–
			1.5709	0.0885				–	2	8	8	–
			2.8161	0.1549				–	–	12	48	–
	19.7608055	1,18,60	0.0013	–	0.0781	0.1348	0.1540	–	–	–	–	–
			1.5710	0.0830				–	2	8	8	–
			2.8161	0.1511				–	–	12	48	–
80	19.9366899	1,19,60	0.0031	–	0.0930	0.1310	0.1580	–	–	–	–	–
			1.6002	0.1195				–	–	12	7	–
			2.8369	0.1429				–	–	12	48	–
	19.9366954	1,20,59	0.0049	–	0.0628	0.0883	0.1355	–	–	–	–	–
			1.6276	0.1198				–	–	12	8	–
			2.8481	0.1447				–	–	12	47	–

Table A.1. (Continued.)

N	E/N	Configuration	r	$\Delta(r)$	f_1	f_2	f_3	$N(3)$	$N(4)$	$N(5)$	$N(6)$	$N(7)$
81	20.1115924	1,20,60	0.0064	–	0.0727	0.0945	0.1006	–	–	–	–	–
			1.6271	0.1021				–	–	12	8	–
			2.8577	0.1372				–	–	12	48	–
	20.1116078	1,20,60	0.0014	–	0.0522	0.1064	0.1124	–	–	–	–	–
			1.6272	0.1176				–	–	12	8	–
			2.8576	0.1262				–	–	12	48	–
82	20.2861031	1,20,61	0.0050	–	0.0420	0.0987	0.1113	–	–	–	–	–
			1.6274	0.1081				–	–	12	8	–
			2.8671	0.1464				–	–	12	49	–
	20.2861622	2,20,60	0.5468	0.0000	0.0699	0.0930	0.1130	–	–	–	–	–
			1.6883	0.1829				–	–	12	8	–
			2.8773	0.1626				–	–	12	48	–
83	20.4598342	2,20,61	0.5447	0.0629	0.0891	0.0971	0.1153	–	–	–	–	–
			1.6886	0.1873				–	–	12	8	–
			2.8866	0.2084				–	–	12	49	–
	20.4598388	2,20,61	0.5457	0.0333	0.0931	0.0993	0.1445	–	–	–	–	–
			1.6887	0.1799				–	–	12	8	–
			2.8865	0.2000				–	–	13	47	1
84	20.6327589	2,21,61	0.5426	0.0047	0.0674	0.0913	0.1289	–	–	–	–	–
			1.7140	0.2477				–	1	10	10	–
			2.9064	0.1758				–	–	12	49	–
	20.6327815	2,21,61	0.5410	0.0353	0.0671	0.1014	0.1031	–	–	–	–	–
			1.7137	0.2052				–	1	10	10	–
			2.9065	0.1568				–	–	12	49	–
85	20.8049075	2,21,62	0.5422	0.0306	0.1124	0.1194	0.1385	–	–	–	–	–
			1.7135	0.2091				–	1	10	10	–
			2.9156	0.1594				–	–	12	50	–
	20.8049198	2,21,62	0.5417	0.0125	0.0962	0.1161	0.1351	–	–	–	–	–
			1.7136	0.2168				–	1	10	10	–
			2.9156	0.1507				–	–	12	50	–
86	20.9765178	2,21,63	0.5403	0.0136	0.0478	0.1128	0.1571	–	–	–	–	–
			1.7138	0.2117				–	–	12	9	–
			2.9247	0.1898				–	–	12	51	–
	20.9765313	2,21,63	0.5407	0.0017	0.0482	0.0972	0.1177	–	–	–	–	–
			1.7137	0.2423				–	1	10	10	–
			2.9247	0.1681				–	–	12	51	–
87	21.1473848	2,22,63	0.5386	0.0063	0.0804	0.1240	0.1480	–	–	–	–	–
			1.7380	0.2213				–	–	12	10	–
			2.9442	0.1553				–	–	13	49	1
	21.1474046	2,22,63	0.5376	0.0097	0.0743	0.0968	0.1314	–	–	–	–	–
			1.7378	0.1895				–	–	12	10	–
			2.9442	0.1573				–	–	12	51	–

Table A.1. (Continued.)

N	E/N	Configuration	r	$\Delta(r)$	f_1	f_2	f_3	$N(3)$	$N(4)$	$N(5)$	$N(6)$	$N(7)$
88	21.3176820	2,22,64	0.5385	0.0081	0.0267	0.1186	0.1367	–	–	–	–	–
			1.7378	0.1826				–	–	12	10	–
			2.9532	0.1602				–	–	12	52	–
	21.3176867	2,22,64	0.5380	0.0000	0.0414	0.1045	0.1146	–	–	–	–	–
			1.7377	0.1946				–	–	12	10	–
			2.9532	0.1176				–	–	12	52	–
89	21.4873691	2,22,65	0.5375	0.0000	0.0990	0.1089	0.1292	–	–	–	–	–
			1.7378	0.1552				–	–	12	10	–
			2.9621	0.1380				–	–	12	53	–
	21.4874019	2,22,65	0.5376	0.012	0.0708	0.1113	0.1208	–	–	–	–	–
			1.7376	0.1962				–	–	12	10	–
			2.9620	0.1646				–	–	12	53	–
90	21.6564037	2,22,66	0.5359	0.0000	0.0791	0.1085	0.1109	–	–	–	–	–
			1.7376	0.1955				–	–	12	10	–
			2.9709	0.1657				–	–	14	50	2
	21.6564542	2,22,66	0.5369	0.0036	0.0674	0.1020	0.1338	–	–	–	–	–
			1.7374	0.2154				–	–	12	10	–
			2.9709	0.1621				–	–	12	54	–
91	21.8248231	3,22,66	0.7050	0.0079	0.1106	0.1150	0.1297	–	–	–	–	–
			1.7916	0.2288				–	–	12	10	–
			2.9891	0.1871				–	–	13	52	1
	21.8248255	2,22,67	0.5363	0.0182	0.0658	0.1152	0.1428	–	–	–	–	–
			1.7373	0.1602				–	–	12	10	–
			2.9797	0.1671				–	–	12	55	–
92	21.9925417	3,22,67	0.7052	0.0304	0.0693	0.1242	0.1369	–	–	–	–	–
			1.7911	0.2386				–	–	12	10	–
			2.9979	0.1984				–	–	12	55	–
	21.9925442	3,22,67	0.7052	0.0264	0.0784	0.1496	0.1600	–	–	–	–	–
			1.7911	0.2187				–	–	12	10	–
			2.9979	0.1873				–	–	12	55	–
93	22.1594897	3,24,66	0.7019	0.0226	0.0269	0.0968	0.1271	–	–	–	–	–
			1.8361	0.2716				–	–	12	12	–
			3.0260	0.1530				–	–	12	54	–
	22.1595122	3,24,66	0.7012	0.0388	0.0585	0.0639	0.0900	–	–	–	–	–
			1.8361	0.2707				–	–	12	12	–
			3.0260	0.1764				–	–	12	54	–
94	22.3258413	3,24,67	0.7001	0.0340	0.0346	0.0906	0.1039	–	–	–	–	–
			1.8356	0.1973				–	–	12	12	–
			3.0347	0.1696				–	–	12	55	–
	22.3258448	3,24,67	0.7006	0.0263	0.0898	0.0970	0.1104	–	–	–	–	–
			1.8354	0.1904				–	–	12	12	–
			3.0347	0.1622				–	–	12	55	–

Table A.1. (Continued.)

N	E/N	Configuration	r	$\Delta(r)$	f_1	f_2	f_3	$N(3)$	$N(4)$	$N(5)$	$N(6)$	$N(7)$
95	22.4918782	4,24,67	0.8089	0.0487	0.0493	0.0944	0.1360	4	–	–	–	–
			1.8848	0.2173				–	–	12	12	–
			3.0522	0.1774				–	–	12	55	–
	22.4918953	4,24,67	0.8090	0.0320	0.0807	0.1119	0.1269	4	–	–	–	–
			1.8846	0.2324				–	–	12	12	–
			3.0523	0.1737				–	–	12	55	–
96	22.6572706	4,24,68	0.8083	0.0572	0.0221	0.0868	0.1205	4	–	–	–	–
			1.8846	0.2237				–	–	12	12	–
			3.0606	0.1854				–	–	12	56	–
	22.6573098	4,24,68	0.8103	0.0277	0.0814	0.1188	0.1338	4	–	–	–	–
			1.8848	0.2344				–	–	12	12	–
			3.0605	0.1997				–	–	12	56	–
97	22.8220322	4,24,69	0.8095	0.0517	0.0736	0.1016	0.1401	4	–	–	–	–
			1.8849	0.2134				–	–	12	12	–
			3.0687	0.2059				–	–	14	53	2
	22.8220678	4,24,69	0.8088	0.0527	0.1019	0.1244	0.1471	4	–	–	–	–
			1.8847	0.2268				–	–	12	12	–
			3.0689	0.1757				–	–	12	57	–
98	22.9861991	4,25,69	0.8081	0.0560	0.0706	0.0706	0.0815	4	–	–	–	–
			1.9055	0.2482				–	–	12	13	–
			3.0864	0.1388				–	–	12	57	–
	22.9862098	4,25,69	0.8078	0.0401	0.0881	0.1184	0.1520	4	–	–	–	–
			1.9058	0.2468				–	–	12	13	–
			3.0863	0.1562				–	–	12	57	–
99	23.1497580	4,25,70	0.8071	0.0581	0.1012	0.1152	0.1281	4	–	–	–	–
			1.9056	0.2477				–	–	12	13	–
			3.0945	0.2070				–	–	12	58	–
	23.1497869	4,25,70	0.8064	0.0276	0.0623	0.1007	0.1264	4	–	–	–	–
			1.9056	0.2638				–	–	12	13	–
			3.0945	0.1858				–	–	13	56	1
100	23.3127593	4,26,70	0.8055	0.0530	0.0710	0.1105	0.1235	4	–	–	–	–
			1.9259	0.3221				–	–	12	14	–
			3.1117	0.2120				–	–	14	54	2
	23.3127595	4,26,70	0.8056	0.0523	0.0946	0.1060	0.1223	4	–	–	–	–
			1.9254	0.2559				–	–	12	14	–
			3.1119	0.2079				–	–	12	58	–

References

[1] Wigner E P 1934 *Phys. Rev.* **46** 1002
[2] Grimes C C and Adams G 1979 *Phys. Rev. Lett.* **42** 795
[3] Andrei E Y, Deville G, Glattli D C, Williams F I B, Paris E and Etienne B 1988 *Phys. Rev. Lett.* **60** 2765
[4] Chu J H and Lin I 1994 *Phys. Rev. Lett.* **72** 4009
[5] Kondo Y, Korhonen J S, Krusius M, Dmitriev V V, Thuneberg E V and Volovik G E 1992 *Phys. Rev. Lett.* **68** 3331
[6] Itano W M, Bollinger J J, Tan J N, Jelenković B, Huang X -P and Wineland D J 1998 *Science* **279** 686
[7] Hornekær L, Kjærgaard N, Thommesen A M and Drewsen M 2001 *Phys. Rev. Lett.* **86** 1994
[8] Arp O, Block D, Piel A and Melzer A 2004 *Phys. Rev. Lett.* **93** 165004
[9] Pohl T, Pattard T and Rost J M 2004 *Phys. Rev. Lett.* **92** 155003
[10] Killian T 2004 *Nature* **429** 815
[11] Rahman A and Schiffer J P 1986 *Phys. Rev. Lett.* **57** 1133
[12] Hasse R W and Schiffer J P 1990 *Ann. Phys. (Berlin)* **203** 419
[13] Schiffer J P 1993 *Phys. Rev. Lett.* **70** 818
[14] Schiffer J P 2002 *Phys. Rev. Lett.* **88** 205003
[15] Dubin D H E and O'Neil T M 1988 *Phys. Rev. Lett.* **60** 511
[16] Gilbert S L, Bollinger J J and Wineland D J 1988 *Phys. Rev. Lett.* **60** 2022
[17] Diedrich F, Peik E, Chen J M, Quint W and Walther H 1987 *Phys. Rev. Lett.* **59** 2931
[18] Arp O, Block D and Piel A 2004 *Phys. Rev. Lett.* **93** 165004
[19] Bonitz M, Block D, Arp O, Golubnychiy V, Baumgartner H, Ludwig P, Piel A and Filinov A 2006 *Phys. Rev. Lett.* **96** 075001
[20] Löwen H 1994 *Phys. Rep.* **237** 249
[21] Kong M, Partoens B and Peeters F M 2003 *New J. Phys.* **5** 23
[22] Hasse R W and Avilov V V 1991 *Phys. Rev.* A **44** 4506
[23] Schiffer J P 2003 *J. Phys. B: At. Mol. Opt. Phys.* **36** 511
[24] Rafac R, Schiffer J P, Hangst J S, Dubin D H E and Wales D J 1991 *Proc. Natl Acad. Sci. USA* **88** 483
[25] Arp O, Block D, Bonitz M, Fehske H, Golubnychiy V, Kosse S, Ludwig P, Melzer A and Piel A 2005 *J. Phys.: Conf. Ser.* **11** 234
[26] Ludwig P, Kosse S and Bonitz M 2005 *Phys. Rev.* E **71** 046403
[27] Schweigert V A and Peeters F M 1995 *Phys. Rev.* B **51** 7700
[28] Bonsall L and Maradudin A A 1977 *Phys. Rev.* B **15** 1959
[29] Kroto H W, Heath J R, Obrien S C, Curl R F and Smalley R E 1985 *Nature* **318** 162
[30] Jarrold M F 2000 *Nature* **407** 26
[31] Pérez-Garrido A, Dodgson M J W and Moore M A 1996 *Phys. Rev.* B **56** 3640
[32] Thomson J J 1904 *Phil. Mag.* **7** 237
[33] Leiderer P 1995 *Z. Phys.* B **98** 303
[34] Marzec C J and Day L A 1993 *Biophys. J.* **65** 2559
[35] Sleytr U B, Sára M, Pum D and Schuster B 2001 *Prog. Surf. Sci.* **68** 231
[36] Pum D, Messner P and Sleytr U B 1991 *J. Bacteriol.* **173** 6865
[37] Dubin D H E and Schiffer J P 1996 *Phys. Rev.* E **53** 5249
[38] Partoens B and Singha Deo P 2004 *Phys. Rev.* B **69** 245415
[39] Earnshaw S 1842 *Trans. Camb. Philos. Soc.* **7** 97
[40] Melzer A 2003 *Phys. Rev.* E **67** 016411
[41] Partoens B and Peeters F M 1997 *J. Phys.: Condens. Matter* **9** 5383
[42] Melzer A, Klindworth M and Piel A 2001 *Phys. Rev. Lett.* **87** 115002
[43] Sheridan T E 2005 *Phys. Rev.* E **72** 026405
[44] Tsuruta K and Ichimaru S 1993 *Phys. Rev.* A **48** 1339
[45] Bedanov V M and Peeters F M 1993 *Phys. Rev.* B **49** 2667